JOURNAL OF MATERIALS SCIENCE 22 (1987) 2305–2308

Fracture toughness of some metallic glasses

V. OCELÍK, P. DIKO, V. HAJKO JR., J. MIŠKUF
Institute of Experimental Physics, Slovak Academy of Sciences, Solovjevova 47, 040 01 Košice, Czechoslovakia

P. DUHAJ
Institute of Physics, Electro-Physical Research Centre, Slovak Academy of Sciences, Dúbravská cesta, 842 28 Bratislava, Czechoslovakia

The critical stress intensity factor of $Fe_{40}Ni_{40}B_{20}$, $Fe_{30}Cr_{10}Ni_{40}B_{20}$, $Ni_{80}Si_{10}B_{10}$ and $Ni_{80}Si_5B_{15}$ metallic glass ribbons was measured. Stressing by ultrasound, a new method for preparation a sharp crack in a metallic glass, was used. Only shear rupture failures was investigated for all alloys.

1. Introduction

From previous papers [1–8] it is seen that the fracture toughness of metallic glasses is significantly influenced by a number of factors, which were briefly summarized by Henderson *et al.* [4]:

1. The thickness of metallic glass specimens lies in the range where it is necessary to prove if the fracture takes place under conditions of either plane stress (vein pattern morphology of the fracture surfaces) or plane strain (cleavage or chevron pattern morphology) or under a combination of both these modes.

2. The various "quenched-in" defects, e.g. oxides, voids etc., must be taken into account.

3. The presence of structural relaxation with time and its influence on the mechanical properties also play an important role.

Scanning electron microscopy (SEM) of fracture surfaces reveals the role of "quenched-in" defects in the process of the failure [4] and also enables specification of the stress conditions in the crack tip under which the fracture takes place.

2. Experimental procedure

The critical stress intensity factor was measured on Fe–Ni–B, Fe–Cr–Ni–B and Ni–Si–B type metallic glass ribbons in the centre-cracked panel configuration [3]. Chemical composition, width $2b$, thickness, Vickers microhardness and results of the X-ray test for amorphousness are shown in Table I. For values of thickness and microhardness the ranges of 95% reliability are also indicated. The difference between the average thicknesses, 36.0 and 36.9 μm, for $Fe_{40}Ni_{40}B_{20}$ ribbons are not significant, but we distinguish them because these two ribbons were prepared at different velocities of quenching wheel.

Specimens were cut from the ribbons and in their centre a circular hole, 0.1 to 0.5 mm diameter, was produced by electric discharge machining.

A sharp crack was produced by high-frequency loading using a longitudinal ultrasonic wave of frequency 22.3 kHz. If the length of the specimen, one end of which is mechanically connected with the source of ultrasound, is equal to the half-wavelength of the stress wave, the specimen is in resonance with the source. Thus the maximum amplitude of the mechanical stress

$$\sigma_m = \Omega A(\varrho E)^{1/2} \quad (1)$$

is produced in the half-length of the specimen, where Ω is the angular frequency, A is the amplitude of oscillation in the junction source-specimen, ϱ is the density and E is Young's modulus of the specimen. If the hole in the specimen, which acts as a stress concentrator, is also situated in this place, suitable conditions exist for the nucleation and growth of the fatigue crack in the direction perpendicular to the longitudinal axis of the specimen. The final length of the crack $2a \approx 0.7$ to 2.3 mm was obtained after 1×10^6 to 3×10^6 cycles with the amplitude $A = 2$ to 3 μm. It

TABLE I Characteristics of the experimental materials

Alloy	Width $2b$ (mm)	Thickness (μm)	HVM	X-ray test*
$Fe_{40}Ni_{40}B_{20}$	9.50	20.3 ± 0.7	815 ± 26	A
	9.55	28.5 ± 1.1	878 ± 26	A
	9.55	36.0 ± 1.1	882 ± 18	A
	9.55	36.9 ± 1.2	873 ± 31	A
$Fe_{30}Cr_{10}Ni_{40}B_{20}$	9.50	18.4 ± 1.1	839 ± 30	A
	9.50	20.2 ± 0.6	812 ± 16	A
$Ni_{80}Si_{10}B_{10}$	10.20	23.1 ± 0.6	637 ± 15	A
$Ni_{80}Si_5B_{15}$	10.20	26.6 ± 0.6	682 ± 11	A+C

*A, only amorphous. A+C, amorphous and crystalline.

0022–2461/87 $03.00 + .12

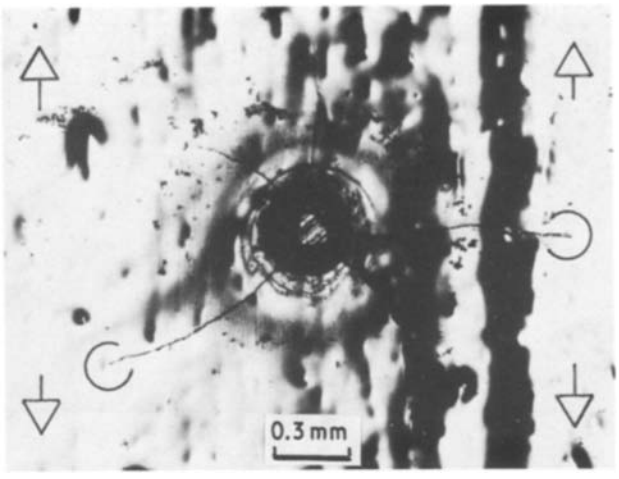

Figure 1 The distribution of the fatigue cracks near the stress concentrator for $Fe_{40}Ni_{40}B_{20}$, 36 μm thick, ribbon.

may be estimated from Equation 1 and using ϱ and E from [9], that the maximum tensile stress $\sigma_m \sim 49$ MPa for $Fe_{40}Ni_{40}B_{20}$ ribbon. Approximately half of the total cycles was used for nucleation. The single crack on both sides of the hole and its propagation in the expected direction was observed in a few cases only. Usually a number of fatigue cracks was observed, one of them gradually becoming dominant and propagating further in the direction perpendicular to the edge of the specimen. Fig. 1 shows this situation for the $Fe_{40}Ni_{40}B_{20}$ specimen, 36 μm thick. The arrows indicate the direction of the mechanical cyclic stressing and the direction of the nominal tensile stress during the measurement of the fracture toughness. Tips of the main crack are designated by the circles and its length in the direction of its expected propagation during the fracture toughness test was measured optically. No slip bands were observed near the fatigue cracks. Thus the time necessary for preparation of one specimen with a sharp crack by ultrasound was not much longer than 2 min.

The tensile tests were carried out on an Instron machine with a strain rate of 2.8×10^{-4} sec^{-1}. For calculation of the values of the critical stress intensity factor, the following formula was used:

$$K_c = \sigma_{fr} Y(\pi a)^{1/2} \quad (2)$$

where σ_{fr} is the nominal stress at fracture and Y is the correction for the finite width of the specimen [6].

3. Discussion

Fractographic analysis of the fracture by SEM TESLA BS 300 and Jeol CF 35 confirmed that the failure of all specimens was caused by shear mechanism with subsequent meniscus instability [10], i.e. by a combination of tearing and opening mode. Thus the measured values of the critical stress intensity factors depend on the specimen thickness [11]. Figs 2a and b show SEM images of the opposite fracture surfaces for the $Fe_{40}Ni_{40}B_{20}$ specimen 36 μm thick in the transition region fatigue–shear failure. These images show a "mirror" similarity of the vein morphology of the opposite surfaces within the shear region. The failure morphology of the other alloys under investigation shows no significant differences from that shown in Fig. 2. Small differences may be found in the size of the smooth region, which is governed by inhomogeneous shear, and also in the density and width of the veins.

Fig. 3a shows the dependence of measured values of the fracture stress on $(\pi a)^{-1/2}$ for all four thicknesses of the $Fe_{40}Ni_{40}B_{20}$ alloy. Fig. 3b shows the same dependence for both thicknesses of the $Fe_{30}Cr_{10}Ni_{40}B_{20}$ alloy as well as for the $Ni_{80}Si_{10}B_{10}$ and $Ni_{80}Si_5B_{15}$ alloys. If the geometrical correction $Y \sim 1$, which is valid for the length of the investigated cracks, the slope of the straight line fitting the experimental values represents the value of K_c.

The dependence of K_c on thickness for the $Fe_{40}Ni_{40}B_{20}$ specimens and the values of this factor for the $Fe_{30}Cr_{10}Ni_{40}B_{20}$ alloy of both thicknesses, as well as for the $Ni_{80}Si_{10}B_{10}$ and the $Ni_{80}Si_5B_{15}$ alloys, are shown in Fig. 4. The range of 95% reliability is also shown, each range being not larger than 5% of the mean value. The measured values of K_c are in good agreement with the results of some previous papers [1, 4, 5, 7, 8]. On the other hand, for similar alloy compositions and similar specimen thicknesses a failure under plane-strain conditions with the values of K_c around 10 MPa m$^{1/2}$ was observed by some authors [2, 3, 6].

As the difference between the plasticity properties

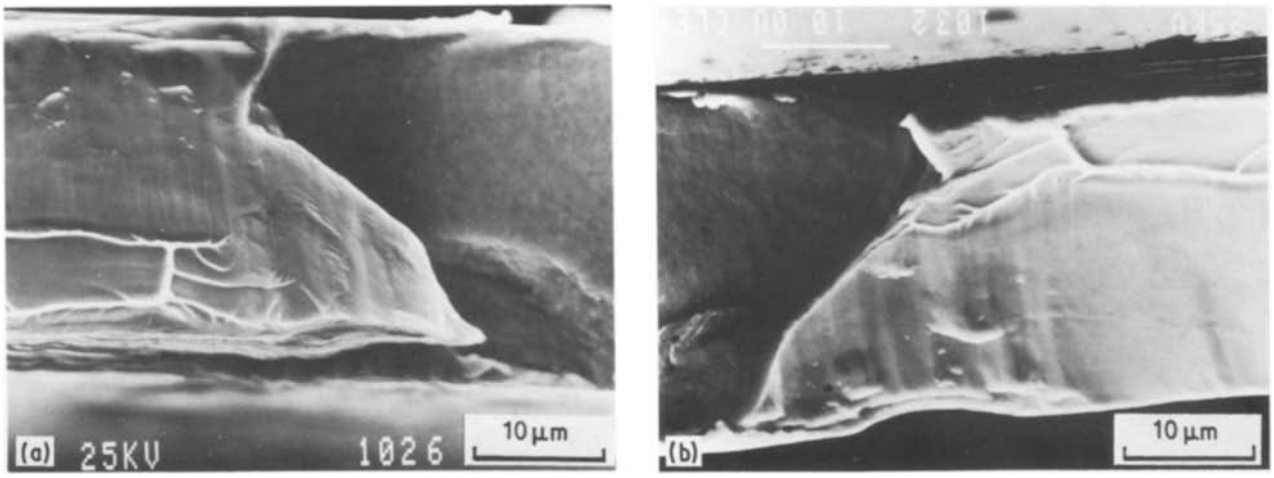

Figure 2 SEMs of the fracture surfaces of the $Fe_{40}Ni_{40}B_{20}$ ribbon exhibiting the transition from the fatigue failure to the shear one. (a) and (b) are matching photographs of the same regions of the fracture.

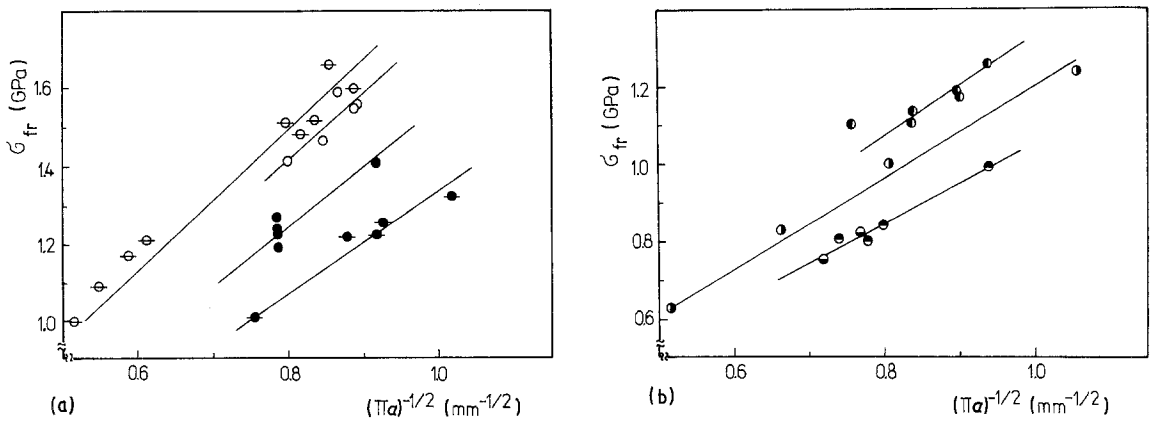

Figure 3 The fracture stress plotted against $(\pi a)^{-1/2}$ for (a) $Fe_{40}Ni_{40}B_{20}$ alloy (○) 36.9 μm, (⊖) 36.0 μm, (●) 28.5 μm, (⊖) 20.3 μm, and (b) (◓, ◒) $Fe_{30}Cr_{10}Ni_{40}B_{20}$, (◑) $Ni_{80}Si_{10}B_{10}$ and (◐) $Ni_{80}Si_5B_{15}$ alloys (◓, 20.2 μm; ◒, 18.4 μm).

of the $Fe_{40}Ni_{40}B_{20}$ specimens prepared at different cooling rates was not confirmed by the values of microhardness (in Table I), the increase of K_c with specimen thickness shown in Fig. 4 may be explained as follows. In thin specimens the condition of plane stress in the crack tip may be expected over the whole specimen thickness. If the thickness increased a triaxial stress appears in the middle of the specimen and this region grows with the further thickness increase. This effect results in the decrease of the value of the shear component of the stress intensity tensor in the middle layer of the specimen. Supposing that the failure in this region is not caused by the normal stress component (in fact, we did not observe it on any specimen), it is necessary to increase the nominal tensile stress in thicker specimens to initiate the shear failure also in their middle layers.

It may be concluded from Fig. 4, that the substitution of one quarter of the iron atoms by chromium atoms in the $Fe_{40}Ni_{40}B_{20}$ alloy leads to the apparent decrease of K_c. However, a similar conclusion about the influence of the different proportion of the metalloid atoms in the Ni–Si–B type alloys cannot be made, because of significant differences in the specimen thicknesses. However, it is interesting to note that the presence of the crystalline phase in the $Ni_{80}Si_5B_{15}$ alloy (see Table I), caused no decrease of toughness in comparison with only amorphous $Ni_{80}Si_{10}B_{10}$ alloy. This crystalline phase consists probably only of the small crystallites formed on the surface during the preparation of the specimens and such surface effects have no influence on the behaviour of the crack tip in the stress field.

Henning *et al.* [6] pointed out the strong dependence of the measured value of K_c on the value of the parameter a/b up to $a/b = 0.3$ also for unstiffened specimens. However, in agreement with Waku and Masumoto [8], such dependence was not confirmed by our measurements, which show a small dispersion for the series of specimens with different initial crack lengths. The subcritical crack growth under gradual loading of the $Fe_{40}Ni_{40}B_{20}$ specimens, 40 μm thick, was also observed by Henning *et al.* [6]. No fractographic evidence of this phenomena was found on any of our specimens.

Stressing by ultrasound was used for the first time to produce a sharp crack in a metallic glass. This method is more efficient than the usual cycle loading in fatigue-test machines with a frequency of about 1 Hz [2]. However, on the other hand, not all specimens prepared by this method show ideal geometrical localization of the crack, but this fact is of little importance, as was confirmed by a low dispersion of K_c values on the samples with quite differently located cracks. However, it may be expected that the eliptical initial hole will cause a better geometrical localization of the crack. A further advantage of this method lies in the fact that fatigue cracks are produced at stresses, which are lower by one order of magnitude than classic loading in fatigue-test machines [2–4]. Therefore, no slip bands are observed near fatigue failure and also the fatigue fracture surface is smoother (compare Figs 2 and 1 in [1]).

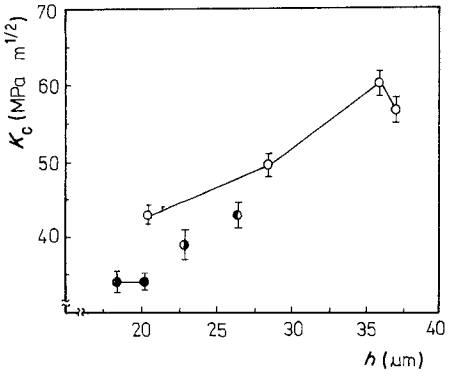

Figure 4 The critical stress intensity factor K_c as a function of thickness for various metallic glasses. (○) $Fe_{40}Ni_{40}B_{20}$, (●) $Fe_{30}Cr_{10}Ni_{40}B_{20}$, (◑) $Ni_{80}Si_{10}B_{10}$, (◐) $Ni_{80}Si_5B_{15}$.

References

1. L. A. DAVIS, *J. Mater. Sci.* **10** (1975) 1557.
2. D. G. AST and D. KRENITSKY, *Mater. Sci. Engng* **23** (1976) 241.
3. L. A. DAVIS, *Met. Trans.* **10A** (1979) 235.
4. S. HENDERSON, J. V. WOOD and G. W. WEIDMANN, *J. Mater. Sci. Lett.* **2** (1983) 375.
5. K. WETZIG, W. POMPE, H. FIEDLER and V. P. ALJOCHIN, *Crystal Res. Technol.* **18** (1983) 1181.
6. W. HENNING, M. CALVO and F. OSTERSTOCK, *J. Mater. Sci.* **20** (1985) 1889.
7. M. CALVO, W. HENNING and F. OSTERSTOCK, Proceedings of the 5th International Conference on Rapidly Quenched metals, Würzburg (1985) pp. 1385–8.
8. Y. WAKU and T. MASUMOTO, Proceedings of the 4th International Conference on Rapidly Quenched Metals,

Sendai (1981) pp. 1395–8.
9. J. C. M. LI, "Ultrarapid Quenching of the Liquid Alloys", edited by H. Herman (Academic Press, London, 1981) p. 325.
10. A. S. ARGON and M. SALAMA, *Mater. Sci. Engng* **23** (1976) 219.
11. J. F. KNOTT, "Fundamentals of Fracture Mechanics" (Butterworths, London, 1973).

Received 21 April
and accepted 11 November 1986